Computers in Biology and Medicine 114 (2019) 103441

Contents lists available at ScienceDirect

Computers in Biology and Medicine

journal homepage: http://www.elsevier.com/locate/compbiomed

Evaluation of synchronization measures for capturing the lagged synchronization between EEG channels: A cognitive task recognition approach

B. Orkan Olcay *, Bilge Karaçalı

Department of Electrical and Electronics Engineering, Izmir Institute of Technology, 35430, Urla, Izmir, Turkey

ARTICLE INFO

Keywords:
EEG
Brain connectivity
Synchronization measures
Cognitive task recognition
FLD
Mutual information
Phase locking value
Cosine based similarity
Cross correlation
Nonlinear interdependency
Cross correntropy

ABSTRACT

During cognitive, perceptual and sensory tasks, connectivity profile changes across different regions of the brain. Variations of such connectivity patterns between different cognitive tasks can be evaluated using pairwise synchronization measures applied to electrophysiological signals, such as electroencephalography (EEG). However, connectivity-based task recognition approaches achieving viable recognition performance have been lacking from the literature. By using several synchronization measures, we identify time lags between channel pairs during different cognitive tasks.

We employed mutual information, cross correntropy, cross correlation, phase locking value, cosine similarity and nonlinear interdependence measures. In the training phase, for each type of cognitive task, we identify the time lags that maximize the average synchronization between channel pairs. These lags are used to calculate pairwise synchronization values with which we construct the train and test feature vectors for recognition of the cognitive task carried out using Fisher's linear discriminant (FLD) analysis.

We tested our framework in a motor imagery activity recognition scenario on PhysioNet Motor Movement/Imagery and BCI Competition-III IVa datasets. For PhysioNet dataset, average performance results ranging between % 51 and % 61 across 20 subjects. For BCI Competition-III dataset, we achieve an average recognition performance of % 76 which is above the minimum reliable communication rate (% 70).

We achieved an average accuracy over the minimum reliable communication rate on the BCI Competition-III dataset. Performance levels were lower on the PhysioNet dataset. These results indicate that a viable task recognition system is achievable using pairwise synchronization measures evaluated at the proper task specific lags.

1. Introduction

Understanding and characterization of dynamically changing features of the brain under various types of sensory, perceptual, cognitive events as well as neural impairments have been the subject of intense research for many years [1–3]. As the main outcome of this research, a BCI system aims to establish an external communication pathway between the brain and the real world that helps to retrieve, among other things, the movement ability of subjects who suffer from motor disabilities [4]. As depicted in many review articles, neurological disorders can impose difficulties on individuals in interacting with their surroundings [5]. In line with technological advances, these systems have become crucial in many areas, especially in rehabilitation technologies [6]. For instance, speller type BCI systems can reactivate the communication ability of people who suffer from speech difficulties by substituting the real pathway with a computerized one [7,8]. Some of the other well-known applications can be listed as wheelchair control that retrieves the movement ability for paralyzed individuals [9], computer control [10], internet surfing [11], deceit identification [12], and implicit intent recognition [13].

In addition to BCI studies, various clinical fields also require monitoring and analysis of gradual changes of the brain functioning. As an example, a sleep stage classification method was proposed for accurate diagnosis and treatment of sleep related disorders [14]. In Ref. [15], the depth of anesthesia (DOA) was evaluated by calculating the complexity of electrophysiological activity. Different methods for identification of

* Corresponding author.
E-mail addresses: bilalolcay@iyte.edu.tr (B.O. Olcay), bilge@iyte.edu.tr (B. Karaçalı).

https://doi.org/10.1016/j.compbiomed.2019.103441
Received 28 May 2019; Received in revised form 25 August 2019; Accepted 7 September 2019
Available online 16 September 2019

epileptic brain activity were proposed in Refs. [16–18]. Dutta et al. proposed a method for recognizing different kinds of cognitive tasks [19]. Besserve et al. proposed a cognitive task performance prediction algorithm to predict mental fatigue [20]. As a general strategy, in these studies, in the training phase, an algorithm extracts salient features from the electrophysiological brain activity and a classification algorithm is trained to provide the highest performance in recognizing the desired activity using these features. In the recognition phase, the classifier decides upon the ongoing brain activity by analyzing and classifying the upcoming features.

In the literature, a great deal of cognitive task recognition approaches uses EEG to analyze the activity of the brain pertinent to cognitive/motor intentions of the participants [21]. The main reasons for choosing EEG for this purpose are its ease of use and harmlessness to the participants. The vast majority of EEG-based motor imagery activity recognition studies use sensorimotor oscillations (SMR) [9] to decode user intentions, offering reliable control of various real-world applications such as robotic arm control [22] and quadcopter control [23]. Commanding a helicopter in a 3D environment was achieved via an SMR based BCI approach [24].

A number of SMR based features (typically found in the 8–30 Hz band) have been proposed in the literature such as the power increase/decrease (i.e. event-related desynchronization (ERD) and event-related synchronization (ERS) features) [25], auto-regressive (AR) model coefficients [26,27], time-frequency based features [28–30], Common Spatial Patterns (CSP) [31] and its variants [32,33]. In addition, topographic voltage distribution [34] and time domain parameters with various derivative orders have been used with some success as features for motor imagery activity recognition [35].

During cognitive, perceptual, and sensory tasks, statistical coupling emerges across different regions of brain, termed as “connectivity” [36]. Brain connectivity phenomenon has been depicted as vital for understanding the modular organization of the brain [37,38]. Two distinct statistical connectivity types are observed in the brain: functional connectivity refers to the temporal linear/nonlinear correlation, and effective connectivity highlights causal interactions between the electrophysiological signals obtained from different brain regions [39]. Particular cognitive states as well as particular neurological disorders give rise to aberration of functional connectivity between electrophysiological signals [40–44].

Synchronization measures have proven to be useful in elucidating the connectivity strength between subsystems to a certain extent. Numerous synchronization measures have been proposed in the literature to assess brain connectivity such as mutual information [45,46], transfer entropy [42,44,47,48], partial mutual information [49], correntropy [50], mean square contingency [51], generalized measure of association (GMA) [52], cosine-based similarity [41], phase locking value [53], and phase lag index [54], and synchronization likelihood [55]. Such a variety in brain synchronization measures can be attributed to a wide-ranging effort to distinguish brain states during different motor or cognitive tasks based on synchronization profiles. Even with a handful of brain regions, pairwise synchrony counts grow quadratically, providing a combinatorial explosion of synchronization profiles based on the presence or absence of synchrony in each pairwise evaluation. In case each brain state associates with a distinct synchronization profile, the number of brain states that can potentially be distinguished from each other is staggering. In spite of this potential, there are relatively few studies that evaluate the performance of different synchronization measures in a cognitive task/state recognition scenario [56–61]. Currently, a limited number of studies exist in the literature that use brain connectivity as a basis for motor imagery activity recognition [62]. Daly et al. obtained phase locking values from the EEG signals by means of an empirical mode decomposition approach to recognize different motor imagery activities [63]. Gonuguntla et al. proposed to classify EEG signals recorded under different stimuli types by constructing task-specific functional interactions in the form of phase locking values of channel pairs [64]. In another study, EEG-based connectivity features were also used as a biomarker for person identification [65]. A cross-correlogram technique was proposed for the recognition of the right hand/foot motor imagery activities [66]. The majority of the synchronization-based cognitive task characterization studies ignore the time lag information between electrophysiological signals. In Ref. [67], using cross-correlation, Hermanto et al. try to recognize motor imagery brain activity by finding the time lags between electrophysiological signal pairs across periods. In here, the main assumption is that the brain generates similar motor imagery related oscillatory activity within same time interval.

In this study, we adopt a new perspective for cognitive task recognition that explores different synchronization measures to capture the task-specific inter-channel time lag between remote brain areas. This approach is based on the premise that during cognitive tasks, selective interactions between distant brain regions arise at a time lag profile that is specific to and characteristic of the task at hand [68–72]. In the literature, there are some studies that exploit the time lag of maximum information transfer in detecting functional impairment in the analysis of brain activity via information theoretic methods [43,73]. In addition, time lag between EEG channels has been used to identify the epileptic foci [74,75]. Van Bergen estimated and analyzed the time lag between EEG signals by utilizing the mutual information [76]. Boeijinga and Lopez da Silva estimated the time lag between EEG channels to identify the propagation direction of beta activity in the cat brain [77]. Adhikari et al. evaluated a study on mice and discovered consistent time lag by applying cross-correlation to envelope of instantaneous amplitudes of local field potentials recorded from medial prefrontal cortex and ventral hippocampus during awake state [78]. All these studies suggest that there is a systematic organization in time lag profiles between distinct areas of the brain during particular cognitive states. If that is the case, brain synchrony between different regions that arise in accordance with cognitive or motor tasks may go undetected by an approach that does not consider the inherent time lag. Indeed, it is highly possible that the conspicuous lack of synchrony-based task recognition studies is due to the inability of establishing the synchrony using methods that disregard this time lag. In order to address this issue, we carried out a comparative evaluation of well-known synchronization measures to assess activity specific time lag organization between EEG channels in a motor imagery activity recognition scenario. This approach can also be easily adapted to analyze other types of cognitive tasks/states. With further adaptations, it can be used on continuously flowing EEG data as required in online BCI applications.

The remainder of this paper is organized as follows: In the Materials and Methods Section, the properties of the EEG datasets used in this study are described, accompanied by an operational flow diagram of the proposed method. Next, the definitions and formulations of coherence measures are provided. In Results, the classification and the novel cross validation schemes are summarized, and performance results obtained via the proposed method are presented. In Discussion, we elaborate on the merits and drawbacks of the approach and the obtained results in comparison with a benchmark method. The final section concludes the study.

2. Materials and Methods

In this section, we first describe the datasets used in this study. Next, the operational pipeline of the proposed method is given, along with the calculation of the activity specific time lag and construction of training and test feature vectors generated from both training and test datasets. Finally, the definitions and formulations of the applied synchronization measures are presented.

2.1. Dataset

In this study, comparative performance evaluations were carried out

on two different motor imagery datasets, BCI Competition-III IVa and PhysioNet Motor Movement/Imagery Dataset. The former dataset comprises EEG recordings of 5 subjects as they perform 140 right hand and 140 right foot imagery activity in a randomized order [79]. This dataset was collected using 118 electrodes according to extended international 10/20 system at a sampling frequency of 1000 Hz [80]. During each trial, subjects performed the imagery activities approximately for 3.5 s. We used the 100 Hz down-sampled version of this dataset.

The latter dataset comprises EEG signals of 109 subjects recorded under real and imaginary motor tasks [81]. EEG signals were collected via a BCI2000 system with 160 Hz sampling frequency [82]. The recording system was international 10/10 system with 64 electrodes. For each subject, the experiment was composed of 14 separate sessions, beginning with two eyes open/eyes closed sessions. The progression of the remaining 12 sessions is given in Table 1.

Each task period lasted 4.1 s, followed by a rest period with a duration of 4.2 s. The graphical demonstration of the task/rest periods is given in Fig. 1. Each session contains a total of 30 mixed blocks of task and rest periods.

In this study, we evaluate the performance of the proposed activity recognition framework using the EEG recordings of right fist versus left fist motor imagery task sessions of the first 20 subjects in the dataset.

As a preprocessing step, for both datasets, we re-referenced the signals to the common average to reduce the effect of volume conduction [44,83,84]. Then, to avoid the phase distortion, we filtered the signals with a finite-impulse response band-pass filter with a passband of 8–30 Hz (see Fig. 2). Using the task initiation indices given in these datasets, we extracted the task periods of the EEG signals with the corresponding task label indicating the type of motor imagery activity.

2.2. Proposed Method for Motor Imagery Recognition

The flow diagram of the proposed method is given in Fig. 3. Details of both training and test phases are given below.

2.2.1. Training Phase

In the *Synchronization Calculation* block, for the task periods of each type of imagery activity, we calculated the synchronization values between EEG signals between each channel pair for different time lags τ running from -125 ms to 125 ms [74]. Then, in the τ_{opt} block, for each type of imagery activity (say *ImgAct1* and *ImgAct2*), the time lag $\tau_{i,j}^{ImgAct1}$ and $\tau_{i,j}^{ImgAct2}$ that maximize the average synchronization value between channels i and j is determined as the activity-specific time lag. For each type of imagery activity, we calculate the inter-channel activity-specific time lags $\tau_{i,j}^{ImgAct1}$ and $\tau_{i,j}^{ImgAct2}$ for each channel pair (i, j) using

$$\tau_{i,j}^{ImgAct1} = \underset{\tau}{\operatorname{argmax}} \left(\frac{1}{N_{ImgAct1}} \sum_{k \in I_{ImgAct1}} D\left(s_{i,k}^{Train}, s_{j,k}^{Train}; \tau \right) \right) \tag{1}$$

and

$$\tau_{i,j}^{ImgAct2} = \underset{\tau}{\operatorname{argmax}} \left(\frac{1}{N_{ImgAct2}} \sum_{k \in I_{ImgAct2}} D\left(s_{i,k}^{Train}, s_{j,k}^{Train}; \tau \right) \right) \tag{2}$$

where k is the index of the period, $I_{ImgAct1}$ and $I_{ImgAct2}$ represent the indices of the respective imagery task periods in the training set, and $N_{ImgAct1}$ and $N_{ImgAct2}$ denote the corresponding number of periods. Furthermore, $s_{i,k}^{Train}$ is the EEG signal from the i^{th} channel of the k^{th} imagery activity period. Note also that $\underset{\rho}{\operatorname{argmax}} q(\rho)$ returns value ρ^* over which the function $q(\cdot)$ is maximized. Finally, $D(s_1, s_2; \tau)$ denotes the synchronization measure of choice that measures the relation between EEG channels s_1 and s_2 evaluated at a time lag τ. Then, in the *Classifier Training for FLD* block, for the subsequent recognition of each imagery activity period k in the training dataset, the feature vector ξ_k that contains synchronization values between EEG signals were constructed at time delays $\tau_{i,j}^{ImgAct1}$ and $\tau_{i,j}^{ImgAct2}$ as

$$\xi_k = \begin{bmatrix} D\left(s_{1,k}^{Train}, s_{2,k}^{Train}; \tau_{1,2}^{ImgAct1}\right) \\ D\left(s_{1,k}^{Train}, s_{3,k}^{Train}; \tau_{1,3}^{ImgAct1}\right) \\ \vdots \\ D\left(s_{M-2,k}^{Train}, s_{M,k}^{Train}; \tau_{M-2,M}^{ImgAct1}\right) \\ D\left(s_{M-1,k}^{Train}, s_{M,k}^{Train}; \tau_{M-1,M}^{ImgAct1}\right) \\ D\left(s_{1,k}^{Train}, s_{2,k}^{Train}; \tau_{1,2}^{ImgAct2}\right) \\ D\left(s_{1,k}^{Train}, s_{3,k}^{Train}; \tau_{1,3}^{ImgAct2}\right) \\ \vdots \\ D\left(s_{M-2,k}^{Train}, s_{M,k}^{Train}; \tau_{M-2,M}^{ImgAct2}\right) \\ D\left(s_{M-1,k}^{Train}, s_{M,k}^{Train}; \tau_{M-1,M}^{ImgAct2}\right) \end{bmatrix} \tag{3}$$

by collecting inter-channel synchronization values calculated at activity-specific time lags from both activities into a column vector. In the expression above, M represents the number of channels ($M = 118$ for BCI Competition-III dataset, $M = 64$ for PhysioNet dataset) providing feature vectors of size $M(M-1) \times 1$. By using the training feature vectors, we calculated the projection vector and bias parameters of the Fisher's linear discriminant classifier given as [85],

$$f(\xi) = \operatorname{sign}\left(w^T \xi + w_0\right) \tag{4}$$

where $\operatorname{sign}(\rho)$ returns -1 when ρ is less than or equal to zero and $+1$ when ρ is greater than zero, w is the linear projection vector that maximizes the criterion function expressed as

$$J(w) = \frac{w^T S_B w}{w^T S_w w} \tag{5}$$

where S_B and S_w are between- and within-class scatter matrices. The projection vector is obtained as

$$w = (\Sigma_{+1} + \Sigma_{-1})^{-1} (\mu_{+1} - \mu_{-1}) \tag{6}$$

where Σ_{+1} and Σ_{-1} are covariance matrices calculated on both type of feature vectors, and μ_{+1} and μ_{-1} are the respective mean feature vectors. The bias term w_0 is found so that it maximizes the classification rate on the training set.

2.2.2. Test Phase

In the *Synchronization Calculation* block, for each task period of interest characterized by EEG signals $s_1, s_2, \ldots, s_M$, we constructed a

Table 1
Content of remaining 12 sessions with real/imagery task.

Task Name	Real Motor Activity Sessions	Imaginary Motor Activity Sessions
Right/Left Fist	3, 7, 11	4, 8, 12
Both Fist/Both Feet	5, 9, 13	6, 10, 14

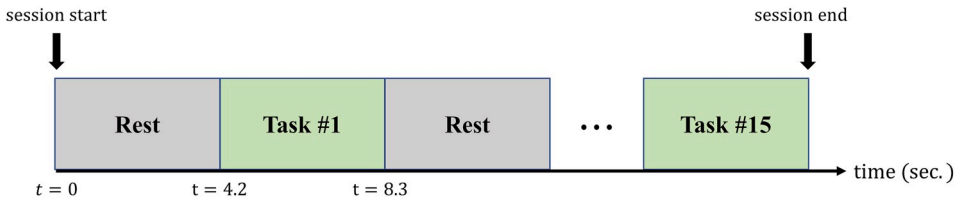

Fig. 1. Illustration of timing diagram of a session with rest and task periods (PhysioNet Dataset).

feature vector ξ using the inter-channel synchronization values calculated at the same activity-specific time lags $\tau_{i,j}^{ImgAct1}$ and $\tau_{i,j}^{ImgAct2}$ and organized into a matching column vector as

$$\xi = \begin{bmatrix} \\ D\left(s_1, s_2; \tau_{1,2}^{ImgAct1}\right) \\ D\left(s_1, s_3; \tau_{1,3}^{ImgAct1}\right) \\ \vdots \\ D\left(s_{M-2}, s_M; \tau_{M-2,M}^{ImgAct1}\right) \\ D\left(s_{M-1}, s_M; \tau_{M-1,M}^{ImgAct1}\right) \\ D\left(s_1, s_2; \tau_{1,2}^{ImgAct2}\right) \\ D\left(s_1, s_3; \tau_{1,3}^{ImgAct2}\right) \\ \vdots \\ D\left(s_{M-2}, s_M; \tau_{M-2,M}^{ImgAct2}\right) \\ D\left(s_{M-1}, s_M; \tau_{M-1,M}^{ImgAct2}\right) \\ \\ \end{bmatrix} \tag{7}$$

In the *Classification Using FLD* block, the imagery activity period in question was then decided upon by carrying out a Fisher's linear discriminant analysis using the formula given in Eq. (4), assigning test feature vectors to either first or second type of imagery activity (i.e. *ImgAct1* or *ImgAct2*).

2.3. Synchronization Measures

The lagged synchronization between EEG channels was calculated using 6 different methods; centered cross-correntropy [86] and mutual information [87], phase locking value [88], cross correlation, nonlinear interdependency [89] and cosine-based similarity [41]. The details of each of these methods are given below. It is important to note that, by using different time lags τ ranging from -125 ms to 125 ms, we calculated the synchronization value between the signals that falls into the time window illustrated with dashed lines in Fig. 4. In the rest of this section, we represent the discretized and delayed signal $y_{i-f_s\tau}$ as y_i^{τ}. Here, τ denotes the time lag, an integer multiple of $^1/_{f_s}$ in milliseconds, and f_s denotes the sampling frequency in Hertz. In Fig. 5, we illustrated the evolution of average synchronization between C3–C4 channels during left fist imagery activity on EEG signals of three sessions of Subject-1 in PhysioNet dataset for varying time lags according to the synchronization measures listed above.

2.3.1. Time-Delayed Cross-Correntropy

In a general sense, correntropy is a measure of similarity that uses both the probability and the time domain structure and evaluates how similar the two signals are simultaneously in these two aspects [90]. The formulation of the cross-correntropy measure between signals X and Y is given in terms of their samples (x_i, y_j) for $i, j = 1, 2, .., N$ as

$$D_{correntropy}(X, Y; \tau) = \frac{1}{N}\sum_{i=1}^{N} \kappa\left(x_i,\ y_i^{\tau}\right) \tag{8}$$

where N is the number of data samples and $\kappa(\cdot,\cdot)$ is the Laplacian kernel function [91] defined as

$$\kappa(z_1, z_2) = \exp(-|z_1 - z_2|) \tag{9}$$

where $\exp(\cdot)$ denotes the exponential function.

2.3.2. Time-Delayed Mutual Information

Mutual information is a well-known measure of how much uncertainty is shared between two processes. The time-delayed mutual information between signals is formulated as

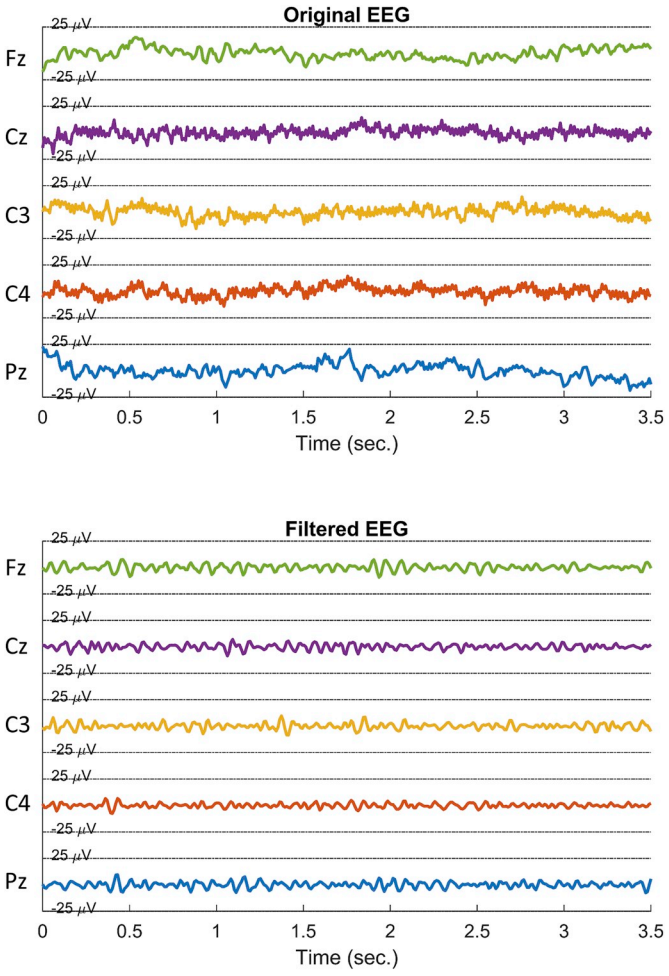

Fig. 2. Illustration of the original EEG signals and the filtered EEG signals of a subject during right hand motor imagery activity (BCI Competition-III dataset).

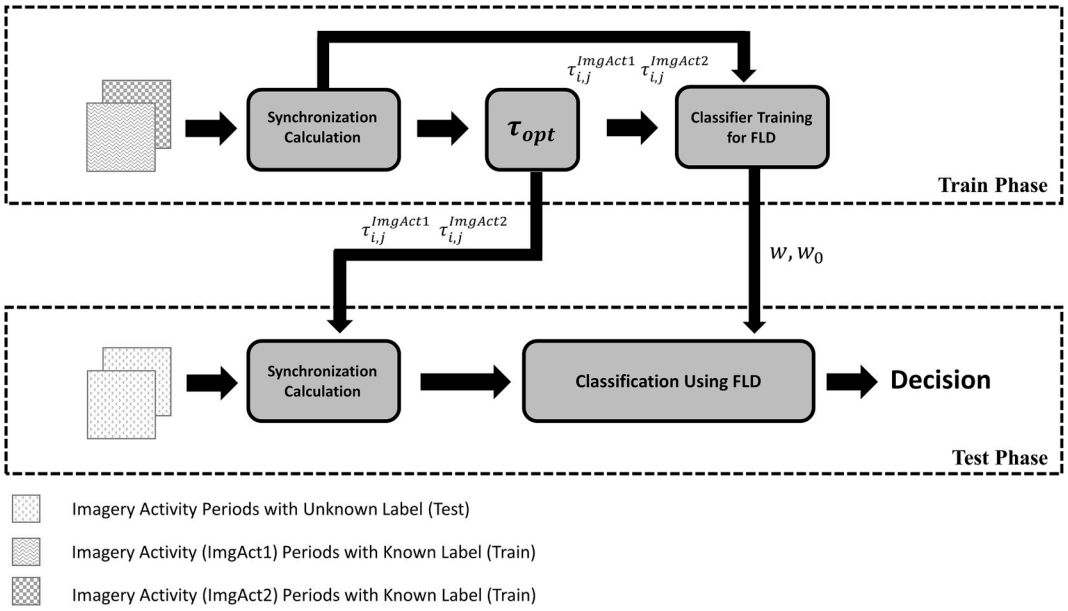

Fig. 3. Flow diagram of the proposed method.

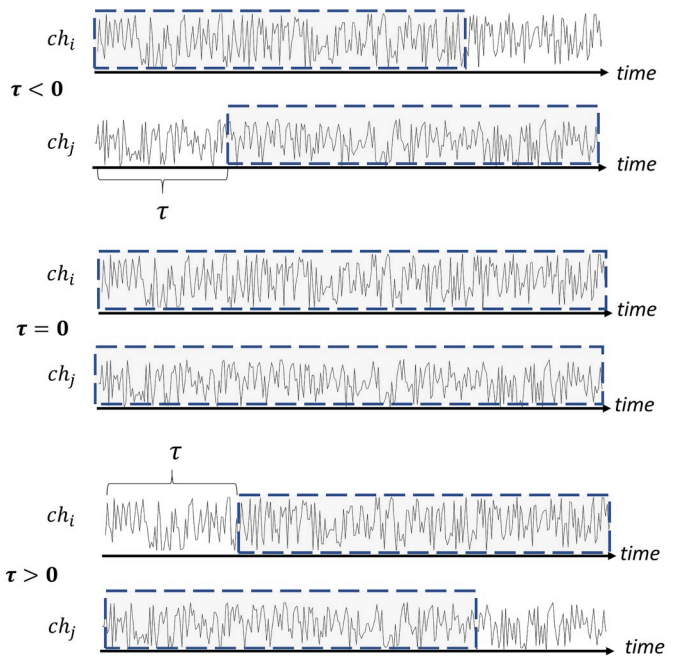

Fig. 4. Time windows from channels ch_i and ch_j used in the calculation of inter-channel synchrony for $\tau < 0$, $\tau = 0$ and $\tau > 0$.

$$D_{MI}(X,Y;\tau) = \int_{-\infty}^{\infty}\int_{-\infty}^{\infty} f_{XY^\tau}(x,y)\,\log\frac{f_{XY^\tau}(x,y)}{f_X(x)\,f_{Y^\tau}(y)}\,dx\,dy \tag{10}$$

where $f_X(x)$ and $f_{Y^\tau}(y)$ are the respective first-order marginal probability densities, and $f_{XY^\tau}(x,y)$ is the corresponding joint probability density. However, obtaining the required probability densities above from a limited number of samples is not straightforward. A common approach is to partition the samples into several bins and calculate histograms. Another strategy is to use kernel-based estimators. Yet, these methods need large sample sets to provide accurate mutual information estimation. As an alternative, Kraskov et al. proposed a method based on neighborhood statistics of the data samples given by

$$D_{MI}(X,Y;\tau) = \psi(k) - \langle \psi(n_x+1) + \psi(n_y+1)\rangle + \psi(N) \tag{11}$$

where $\psi(\cdot)$ is the digamma function [92]. The parameters n_x, n_y denote the number of points whose distances are less than $\varepsilon(i)/2$ to points x_i and y_i^τ respectively, while $\varepsilon(i)/2$ is the maximum of the Euclidean distance between x_i and y_i^τ and their k^{th} neighbor, N is the number of samples, and $\langle\cdot\rangle$ represents the calculation of average over i.

2.3.3. Phase Locking Value

Basically, PLV calculates the stability of the phase difference between two oscillations [88] by averaging the instantaneous phases across trials. The instantaneous phases are calculated by taking the Hilbert transform of the signals. For a signal $x(t)$, its Hilbert transform is defined as

$$\tilde{x}(t) = \frac{1}{\pi}\,PV\int_{-\infty}^{\infty}\frac{x(t')}{t-t'}\,dt' \tag{12}$$

where PV indicates the Cauchy Principal Value. The instantaneous phase of the signal $x(t)$ can then be calculated using

$$\theta_x(t) = \arctan\left(\frac{\tilde{x}(t)}{x(t)}\right) \tag{13}$$

In our analysis, we characterized the phase locking value between channels i and j in a given frame using

$$D_{PLV}(X,Y;\tau) = \frac{1}{N}\left|\sum_{i=1}^{N}\exp\left\{j\left(\theta_{x_i} - \theta_{y_i^\tau}\right)\right\}\right| \tag{14}$$

where N is the common signal length and θ_{x_i} and $\theta_{y_i^\tau}$ represent the instantaneous phases of the corresponding signals [63,64,93]. The PLV equals 1 if the phase difference is constant, and 0 when the phase difference shows a random distribution across trials.

2.3.4. Cross-Correlation

Cross-correlation is the measure of the linear dependence between two variables X and Y. The sample estimate of the cross-correlation can be calculated using

$$D_{xcorr}(X,Y;\tau) = \frac{1}{N - f_s\tau}\sum_{i=1}^{N-f_s\tau} x_i y_i^\tau \tag{15}$$

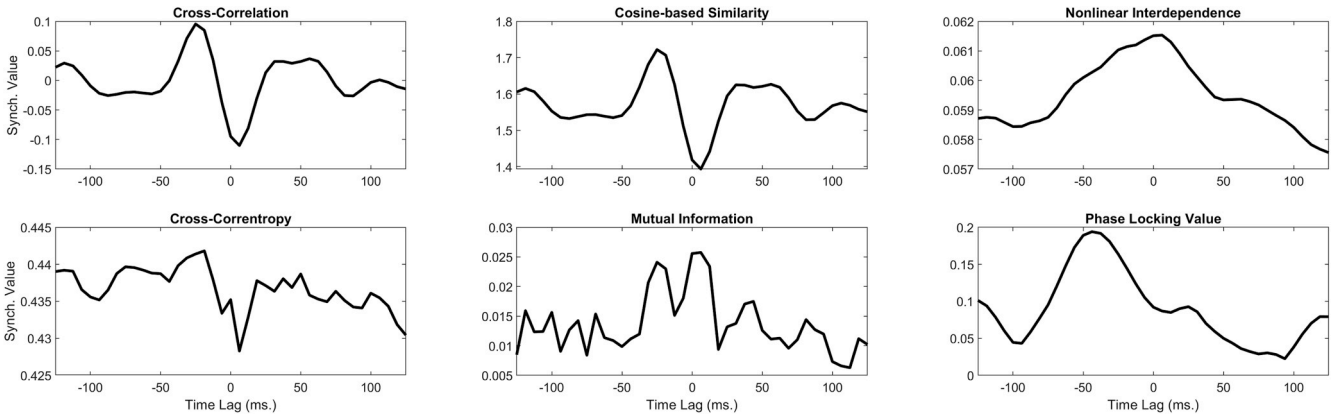

Fig. 5. The time lag versus average synchronization value of all six methods included in this study for the C3–C4 pair of Subject-1 (left fist imagination-PhysioNet Dataset).

The sign of the cross-correlation is an indicator of the direction of the correlation. In this study, we take the absolute value of the resulting correlation value to find the activity-specific time lags based on magnitude only.

2.3.5. Nonlinear Interdependency

Consider the time series data of the signals X and Y collected into phase space vectors $\boldsymbol{x_i} = (x_i, x_{i-d}, \ldots, x_{i-(m-1)d})^T$ and $\boldsymbol{y_j} = (y_j, y_{j-d}, \ldots, y_{j-(m-1)d})^T$ where m and d represent the phase space dimension and the time delay defined in phase space, respectively, and x_i and y_j are the samples of the time series. Then, the average Euclidean distance between n^{th} phase space vector of observation X and its first k nearest neighbors is given as

$$R_n^k(X) = \frac{1}{k}\sum_{p=1}^{k} \left\|\mathbf{x_n} - \mathbf{x_{r_{n,p}}}\right\|^2 \tag{16}$$

where $r_{n,p}$ represents the indices of the nearest neighbors of n^{th} phase space vector of observation x_i and $\|\cdot\|$ is the Euclidean norm. Likewise, the Y^τ -conditioned average Euclidean square distance to its k nearest neighbor of the vectors of observation X is

$$R_n^k(X|Y^\tau) = \frac{1}{k}\sum_{p=1}^{k} \left\|\mathbf{x_n} - \mathbf{x_{s^\tau_{n,p}}}\right\|^2 \tag{17}$$

where Y^τ is the delayed version of Y, and $s^\tau_{n,p}$ denotes the indices of the nearest phase space vectors of Y^τ. Then, the nonlinear interdependence measure between the time series X and Y [89] is defined as

$$D_{nonlinear\_int}(X, Y; \tau) = \frac{1}{N}\sum_{n=1}^{N} \frac{R_n^k(X)}{R_n^k(X|Y^\tau)} \tag{18}$$

By construction, $R_n^k(X|Y^\tau) \geq R_n^k(X)$, so the result is between 0 and 1. The parameter N denotes the sample size. In this study, we selected k as 10, dimension m of phase space vectors as 6, and delay for phase space representation as 1 as initially suggested by Bandt and Pompe [94–96].

2.3.6. Cosine-based Similarity

This synchronization measure calculates and subtracts the angle between two signal vectors from π [41], providing

$$D_{cosine}(X, Y; \tau) = \pi - \arccos\left(\frac{\langle x, y^\tau\rangle}{||x||||y^\tau||}\right) \tag{19}$$

where $\langle\cdot,\cdot\rangle$ and $\|\cdot\|$ represent the inner product and the norm operators respectively. The maximum synchronization between signals occurs when the angle between them is zero.

3. Results

In order to determine the way in which recognition performance varies in response to varying size of the training set, we chronologically partitioned the dataset in two different ways as follows:

- In scenario-1, for PhysioNet dataset, imagery activity periods in session-4 were used for training, imagery activity periods in session-8 and session-12 were used for testing purposes. For BCI Competition-III dataset, the first 94 imagery activity periods were used for training, and the remaining 186 imagery activity periods used for testing purposes. For each dataset, this corresponds to using the first %33,3 of total imagery activity periods for training, and the remaining %66,7 of total imagery activity periods for testing.
- In scenario-2, for PhysioNet dataset, imagery activity periods in session-4 and session-8 were used for training while imagery activity periods in session-12 were used for testing purposes. For BCI Competition-III dataset, the first 186 imagery activity periods were used for training, and the remaining 94 imagery activity periods used for testing. For each dataset, this corresponds to using the first %66,7 of total imagery activity periods for training, and the remaining % 33,3 for testing.

Note also that this kind of partitioning of the data in training and test sets is also more realistic compared to a typical n -fold cross validation scheme with randomly selected training and test sets, since training naturally precedes testing in real applications. In addition, it is also useful to evaluate how much improvement can be expected by increasing the amount of training data.

Prior to classifier construction, to reduce the dimensionality, we have applied feature selection according to each feature's Fisher ratio [97], defined as

$$F_j = \frac{|\mu_{+1,j} - \mu_{-1,j}|}{\sigma_{+1,j} + \sigma_{-1,j}} \tag{20}$$

where $\mu_{+1,j}$, $\mu_{-1,j}$ and $\sigma_{+1,j}$, $\sigma_{-1,j}$ represent the mean and standard deviation of the feature indexed by j on both classes, with $j = 1, \ldots, M(M-1)$. In each chronological cross validation scenario, we selected the features that had higher Fisher ratio values than the mean plus two times the standard deviation of all Fisher ratios across all features. For each scenario, the average classification performance results over 20 subjects from the PhysioNet dataset and the average performance over all 5 subjects of BCI Competition-III dataset are given in Table 3 and Table 4.

For comparison purposes, we also evaluated the recognition performance using a priori selected channel pairs that were identified to be meaningful for right hand versus left hand imagery activity

discrimination in previous EEG connectivity-based studies. Krusienski et al. has proposed to use 9 channels (producing 36 channel pairs) to elucidate the merits and drawbacks of the phase locking value (PLV) method for imagery activity recognition [61]. The performance of additional electrode subsets were also compared for PLV-based activity recognition [98]. Daly et al. argued for the importance of using all spatial and spectral information in the connectivity-based BCI framework which amounts to using all channel pairs [63]. Wang et al. also proposed using a large number of electrode pairs to couple up the motor-activity related brain regions for activity recognition [99]. Rathee et al. proposed three channel pairs arguably offering the greatest contribution for right hand/left hand imagery activity recognition [100]. Hamedi et al. identified additional channel pairs for right- and left-hand imagery activity recognition [101]. These a priori channel pairs are listed in Table 2. Note, however, these channels/channel pairs were identified for right fist versus left fist recognition; thus we applied them for performance evaluation on PhysioNet dataset only and not on BCI Competition dataset as it contains right hand versus right foot imagery activity periods. A similar analysis using a priori selected channels for right hand/right foot recognition was not possible as a comparable list of channels that discriminate between right hand and right foot activities is lacking from the literature. In Ref. [102], authors identified EEG channel networks for BCI Competition-III IVa dataset claimed to be highly discriminative for right foot/right hand motor imagery activity. However, these channel networks are highly subject and frequency specific, and thus, not viable for performance comparison across different subjects (see Ref. [102] and Table I therein). As a result, we did not include these channels. The performance results obtained using these a priori selected right hand versus left hand connectivity features are also given in Tables 3 and 4 for scenario-1 and scenario-2 respectively.

Finally, we compared the performance of the cognitive task recognition framework evaluating the various synchronization measure with a well-known BCI strategy, CSP [31]. In the training phase, we filtered the signals with 8–30 Hz FIR band-pass filter and obtained the CSP filter ($m = 3$). We then applied the CSP filter on both training and test periods. We extracted the log-variance features from CSP-filtered activity periods for recognition purpose. The classification was evaluated again using a FLD analysis. We demonstrate the average performance results in Table 5.

4. Discussion

The immediate observation on the results in Tables 3 and 4 is the stark discrepancies between the recognition performances achieved on the PhysioNet and BCI Competition-III IVa datasets. Based on the performance evaluation criteria proposed by Müller [103], this appears to be a common trait of the PhysioNet dataset as observed in similar studies that report results only on a limited, well-performing subset of the subjects (Table 6) [104–108]. While this can be justified to a certain extent by arguing that poor-performing subjects belonged to a presumed BCI-illiterate category, it falls at odds with the original premise of independent experimental validation. Our results, however, have been obtained from the first 20 subjects in PhysioNet dataset, without any performance-related exclusion criteria in order to avoid such controversies.

Average performances on BCI Competition-III dataset given in Table 3 (in Scenario-1) reveals that mutual information method can better capture the task specific time lags when the size of the training dataset is small. However, with a larger training dataset, cosine-based similarity captured the task specific time lags more accurately and achieved the best average performance on both PhysioNet and BCI Competition-III datasets (see Table 4). Performance of both mutual information-based and cosine similarity-based methods for both scenarios for different BCI Competition-III subjects shown in Table 7 indicate that for three well-performing subjects, the recognition accuracies are in the %70-%90 interval, while the accuracies for the other two is around %60-%65.

To see the ranking of the proposed method, by using original train and test dataset sizes given in the competition website, we also compared our recognition performances with performances given in the BCI Competition-III winner tables (performance rankings are given in the competition website). The mutual information-based and cosine-based activity recognition method ranked the seventh place and eleventh places respectively.

Note that, further improvements may be expected on the recognition performance with additional efforts such as elimination of the background activity or using tailored spatial filters [109]. The average performance can also improve with the size of the training set (BCI Competition-III dataset contains more imagery activity periods than PhysioNet dataset). This suggests that using larger training sets or longer training sequences may lead to better learning and a higher recognition rate than reported here.

In this study, our main aim was to highlight the potential of the inter-channel activity specific time lags in a cognitive task recognition scheme. The feature vectors constructed using these activity-specific time lags were expected to be an indicator of the dichotomy between different cognitive tasks (right/left hand motor imagery for PhysioNet, right hand/right foot for BCI Competition-III dataset). In that spirit, we used FLD analysis as a benchmark classifier. However, for the highest recognition performance, more sophisticated classification methods such as support vector machine (SVM) [110], extreme learning machine [111], kernel based extreme learning machine [112] or sparse Bayesian learning machine classifiers [113] can certainly be evaluated.

Yet, an extended analysis involving linear and nonlinear SVM classifiers on both Scenario-1 and Scenario-2 that we have carried out reveals interesting results (please see Table 8 and Table 9 below). Linear SVM outperformed the FLD analysis, especially on the BCI Competition-III dataset, in all synchronization measures while performance dropped using a radial basis function kernel. Note that, in this analysis, the kernel width parameter σ for nonlinear SVM is calculated as

$$\sigma = \sqrt{\frac{1}{L(L-1)} \sum_{i=1}^{L-1} \sum_{j=i+1}^{L} \left\| \xi_i - \xi_j \right\|^2} \tag{21}$$

where L is the total number of training feature vectors ξ_i, $\|\cdot\|$ represents Euclidean norm. This suggests that a linear classification approach is more reliable in this instance, potentially due to high number of features against a low number of training samples. Furthermore, a clear superiority of linear maximum margin classification on FLD analysis indicates that the generalization ability of FLD analysis is hampered when training samples are low in number, possibly due to the inability to calculate class covariance matrices with sufficient accuracy.

Table 2
The a priori selected channel pairs given in previous studies for right fist/left fist recognition.

	Number of Pairs	Number of Channels	Channels/Channel Pairs
Krusienski et al.	36	9	[T7, F3, P3, C3, Cz, C4, P4, F4, T8]
Wei-CW et al.	45	10	[C5, FC3, CP3, C3, C1, C2, C4, FC4, CP4, C6]
Wei-CB1 et al.	25	10	[C5, FC3, CP3, C3, C1] ↔ [C2, C4, FC4, CP4, C6]
Wei-CB2 et al.	50	15	[AFz, Fz, FCz, F1, F2] ↔ [C5, FC3, CP3, C3, C1], [AFz, Fz, FCz, F1, F2] ↔ [C2, C4, FC4, CP4, C6]
Wang et al.	3	3	[FCz, C3, C4]
Rathee et al.	3	5	[CP1 ↔ C4], [C3 ↔ FC1], [C4 ↔ Cz]
Hamedi et al.	5	6	[C3 ↔ C4], [C1 ↔ Cz], [C2 ↔ Cz], [C1 ↔ C2], [C2 ↔ CPz]

Table 3
The average % performance results of subjects for different datasets for Scenario-1. The rows marked with an asterisk represents the a *priori* selected channel pairs (Right/Left Hand) from the literature.

		Mutual Information	Cosine-Based Similarity	PLV	Nonlinear Interdep.	Cross Correlation	Cross Correntropy
PhysioNet Motor Imagery Dataset (Right/Left Fist Imagery)	Fisher ratio	58,33 ± 10,57	56,83 ± 10,17	54,67 ± 10,83	57 ± 11,44	55,67 ± 8,02	56,16 ± 15,07
	*Krusienski,2012	53,83 ± 10,66	54,16 ± 8,15	55,16 ± 11,96	53 ± 7,1	51,67 ± 8,95	53,17 ± 10,45
	*Wei-CW, 2007	54 ± 13,35	54,67 ± 9,75	53,67 ± 10,97	56,16 ± 12,29	59,83 ± 11,96	56,67 ± 9,85
	*Wei-CB1, 2007	53,67 ± 6,65	54,33 ± 10,71	51,33 ± 8,94	54 ± 6,89	53,5 ± 9,07	52,5 ± 7,78
	*Wei-CB2, 2007	58,5 ± 9,14	52,33 ± 10,71	53,5 ± 10	53,33 ± 8,71	54,5 ± 9,74	50,83 ± 9,48
	*Wang, 2006	53,17 ± 6,7	55,33 ± 8,67	54,83 ± 8,12	52,16 ± 8,67	53,5 ± 9,39	53,17 ± 11,67
	*Rathee, 2017	55 ± 10	53,17 ± 11,41	54,83 ± 8,94	52 ± 10,39	56,5 ± 11,21	54,67 ± 9,32
	*Hamedi, 2016	53,33 ± 9,97	50,5 ± 6,76	52,83 ± 9,13	51,83 ± 9,08	54 ± 6,89	53,16 ± 9,64
BCI Competition III	Fisher ratio	76,69 ± 12,88	70,52 ± 9	68,08 ± 8,7	72,55 ± 9,65	72,65 ± 8,77	75,95 ± 11,56

Table 4
The average % performance results of subjects for different datasets for Scenario-2. The rows marked with an asterisk represents the a *priori* selected channel pairs (Right/Left Hand) from the literature.

		Mutual Information	Cosine-Based Similarity	PLV	Nonlinear Interdep.	Cross Correlation	Cross Correntropy
PhysioNet Motor Imagery Dataset (Right/Left Fist Imagery)	Fisher ratio	59,33 ± 15,12	61 ± 10,2	59,67 ± 15,06	60,67 ± 13,83	60,33 ± 15,37	59,33 ± 16,17
	*Krusienski, 2012	58,67 ± 13,26	56 ± 13,22	57,67 ± 17,34	57,33 ± 15,2	57,33 ± 12,12	55,67 ± 11,9
	*Wei-CW, 2007	51 ± 20,55	57 ± 15,81	56,67 ± 16,11	55,67 ± 17,06	58,67 ± 12,34	51,67 ± 21,61
	*Wei-CB1, 2007	55,33 ± 15	52 ± 11,15	53,33 ± 10,59	56,67 ± 13,42	54,67 ± 13,08	48,33 ± 12,4
	*Wei-CB2, 2007	55 ± 8,88	53,33 ± 16,32	56 ± 13,74	55,33 ± 16,9	53 ± 10	58,33 ± 16,31
	*Wang, 2006	47,33 ± 15,43	56,33 ± 11,94	54,67 ± 12,9	54,67 ± 12,72	54 ± 8,62	56,33 ± 15,51
	*Rathee, 2017	54,33 ± 15,48	55,33 ± 14,36	50 ± 10,92	53,33 ± 14,66	56 ± 12,86	55,33 ± 17,58
	*Hamedi, 2016	51 ± 11,9	54,3 ± 10,65	51,33 ± 10,61	51,67 ± 13,48	53,67 ± 10,91	52,67 ± 11
BCI Competition III	Fisher ratio	75,76 ± 12,3	76 ± 8,43	68,41 ± 11,98	70,73 ± 8,79	68,83 ± 9,72	72 ± 13,07

Table 5
Comparison of average performances (Our method versus CSP).

Method	PhysioNet Dataset		BCI Competition-III Dataset	
	Scenario-1	Scenario-2	Scenario-1	Scenario-2
CSP (m = 3)	% 53,83 ± 4,87	% 55,65 ± 9,97	% 82,33 ± 11,46	% 84,67 ± 15,38
Our method (Cosine-based)	% 56,83 ± 10,17	% 61 ± 10,2	% 70,52 ± 9	% 76 ± 8,43

Table 6
Performance demonstration styles of studies that use the PhysioNet dataset.

Author	Proposed Method	Performance Demonstration Style
Park et al. [104]	Augmented Complex CSP	Eliminates subjects with performance below the %64
Handiru et al. [106]	Optimized Bi-Objective Chan. Selection Method	Uses 35 best performing subjects
Athif et al. [108]	Wavelet transform and CSP filtering based method	Eliminates subject with performance below the %64
Kim et al. [105]	Complex CSP with Strong Uncorrelating Transformation	Eliminates subjects with performance below the %64

Table 7
Individual performances of BCI Competition-III subject for Scenario-1 and Scenario-2. The subjects *al, aw* and *ay* are the well-performing subject.

Subject	Scenario-1		Scenario-2	
	Mutual Information	Cosine-Based Similarity	Mutual Information	Cosine-Based Similarity
aa	% 64,36	% 67,55	% 70,52	% 73,68
al	% 90,95	% 82,97	% 92,63	% 84,21
av	% 62,23	% 60,1	% 64,21	% 64,21
aw	% 79,78	% 65,95	% 66,31	% 73,68
ay	% 86,17	% 76,06	% 84,21	% 84,21

In this study, we tested our framework with two datasets having 160 Hz. (PhysioNet) and 100 Hz. (BCI Competition-III) sampling frequencies. Note that, the sampling frequency of the EEG signals constitutes a fundamental limitation for the method that calculates and uses the inter-channel time lags that emerge between EEG signals during particular cognitive tasks. Actually, it is possible that the true inter-channel time lags deviated from those calculated by the synchronization measures evaluated here due to the low sampling frequency. It is clear that, increasing the sampling frequency may be expected to lead to an increase in the accuracy of the activity-specific time lags that emerge between channels are calculated, as it would provide more data points for the calculation. However, it should also be noted that a higher sampling frequency would cause dramatic increase in computation time. In this study, even for a low sampling frequency, we showed that the inter-channel time lags that maximizes the average synchronization values for each EEG channel pairs (i.e. activity-specific time lags), have potential in characterizing the cognitive activity during a task period. Another limitation, the present framework disregards the subject-specific frequency bands. In general sense, filter bank strategy overcomes the subject-specific frequency band identification problem by incorporating different band-pass filters and identifies most discriminative frequency-specific features before the classification [33,114,115]. For our framework, instead of using 8–30 Hz frequency band, a filter bank structure can be included into the method before the determination of activity-specific time lags. This enables us to calculate and use the frequency-resolved activity-specific time lags may also be expected to improve the recognition performance, albeit in expense of computation time [116]. Still, once the salient subject-specific frequency bands are determined, activity-specific time lags can easily be

Table 8
The comparison of the classification methods for Scenario-1.

		Cosine	Cross Corr.	Nonlinear Int.	Correntropy	Mutual Information	PLV
FLD	PhysioNet	56,83 ± 10,17	55,67 ± 8,02	57 ± 11,44	56,16 ± 15,07	58,33 ± 10,57	54,67 ± 10,83
	BCI Comp.	70,52 ± 9	72,65 ± 8,77	72,55 ± 9,65	75,95 ± 11,56	76,69 ± 12,88	68,08 ± 8,7
Linear SVM	PhysioNet	57,83 ± 10,38	58,17 ± 10,73	50,17 ± 2,28	50,17 ± 9,93	58,5 ± 10,78	60,5 ± 10,99
	BCI Comp.	74,46 ± 9,52	72,97 ± 10,93	77,65 ± 11,89	77,34 ± 9,5	77,97 ± 10,35	70,31 ± 10,58
Nonlinear SVM (RBF Kernel)	PhysioNet	58,83 ± 11	55,83 ± 11,54	58,16 ± 9,58	55,67 ± 14,71	59,83 ± 9,33	58,83 ± 10,21
	BCI Comp.	71,7 ± 8,07	72,12 ± 8,33	76,38 ± 12,36	77,02 ± 8,42	75 ± 10,52	69,78 ± 8,22

Table 9
The comparison of the classification methods for Scenario-2.

		Cosine	Cross Corr.	Nonlinear Int.	Correntropy	Mutual Information	PLV
FLD	PhysioNet	61 ± 10,2	60,33 ± 15,37	60,67 ± 13,83	59,33 ± 16,17	59,33 ± 15,12	59,67 ± 15,06
	BCI Comp.	76 ± 8,43	68,83 ± 9,72	70,73 ± 8,79	72 ± 13,07	75,76 ± 12,3	68,41 ± 11,98
Linear SVM	PhysioNet	59,33 ± 16,02	61,67 ± 14,8	51 ± 10,43	62,33 ± 16,51	59,33 ± 14,96	59,67 ± 15,36
	BCI Comp.	79,57 ± 9,52	77,26 ± 9,75	81,05 ± 8,93	80,21 ± 10,35	81,89 ± 11,8	75,15 ± 13,03
Nonlinear SVM (RBF Kernel)	PhysioNet	58,67 ± 12,53	58,66 ± 14,28	62 ± 13,36	65,33 ± 17,91	59,67 ± 15,21	60 ± 14,82
	BCI Comp.	74,73 ± 5,47	74,1 ± 4,85	78,1 ± 7,85	80 ± 6,69	77,89 ± 10,26	70,94 ± 8,1

calculated and used for subsequent recognition purposes [117].

In the present study, we aimed to determine the most powerful synchronization method among six different methods that captures the most appropriate time lag (activity-specific time lag) between EEG channels that the synchronization (evaluated at this lag) is characteristic to the particular cognitive tasks. In the literature, many different synchronization measures were proposed and subjected to performance comparison using various types of synthetic and real datasets collected under various experimental conditions [56,59,118,119]. However, the main outcome of these studies indicates that there is no universal synchronization measure that works better than all others. It appears a general consensus that different measures calculate the synchronization by taking different feature types of the input signals into consideration [56,57]. During cognitive tasks, the brain presents dynamically changing electrophysiological characteristics and also, the functional connectivity between distant regions are affected from these dynamical changes. Each of the different synchronization methods used in this study attempts to find the activity-specific time lags between electrophysiological signals as captured by the method itself. Since each method evaluates a different aspect of the signals, it is not surprising to observe dissimilar time lags. In the absence of full knowledge of exact time lags between the signals, it is impossible to tell which method is more accurate in calculating the time lag of interest.

In addition to those evaluated in this study, further synchronization estimation methods exist in the literature. Notably, the transfer entropy has been frequently used in both sensor space and source space connectivity studies [42,44,47,72,120,121]. However, due to the high computational requirements during its calculation, transfer entropy does not appear to be a viable method for brain activity recognition. As a result, it was not included in this work. Even then, calculating the mutual information, correntropy and nonlinear interdependency measures for 20 subjects in PhysioNet dataset and 5 subjects for BCI Competition-III dataset took several days. However, for PhysioNet dataset, the required computation time for cross-correlation and cosine-based similarity are about 15,6 s and 13,7 s per subject, respectively. As for BCI Competition-III dataset, for 5 subjects, the corresponding computations took 154,7 s and 202,2 s per subject. While these computation times are not extensive, with the high speed and parallel computing architectures, cosine similarity-based measure stands out as the more practical synchronization evaluation method for a real time cognitive status analysis.

The recognition performance results for the PhysioNet dataset, given in both Tables 3 and 4, shows that we did not achieve the minimum reliable communication rate (%70). These low performances may be due to relatively small training sample size or low-quality of EEG recordings. For the small sample size problem of FLD and/or SVM classifiers, increasing the number of training samples may require long training sequences which then very tiring and therefore challenging for the participants. Pooling and using informative feature vectors from all other subjects may also improve the classification performance of the proposed framework. Y. Jiao et al. proposed sparse group representation method (SGRM) to reduce the required training time without any performance degradation for motor imagery brain computer interface approaches [122]. Briefly, this method identifies and uses informative feature vectors (also features) from a dictionary matrix constructed using both non-target subjects' and target subject's training feature vectors. For our study, as proposed in Ref. [122], exploiting the informative features and feature vectors obtained from both target and non-target subjects' training task periods (for each subject, feature vectors are constructed via inter-channel synchronization values evaluated at activity-specific time lags) may improve the recognition performances especially obtained for PhysioNet dataset. Similar sparse representation approach for frequency-resolved informative feature identification was proposed and can be applied to our framework [123]. Another problem, since we don't accurately know when the subject begins and ends the imagination of the motor movement task, we used whole task period EEG signals to calculate the activity-specific time lags. For an accurate brain activity characterization, an extended approach that jointly optimizes the time window and the frequency band can also be adopted in our framework before the inter-channel activity-specific time lag estimation [124].

For both PhysioNet and BCI Competition-III datasets, we listed the electrode pairs that provide meaningful differences between two cognitive tasks along with five most significant electrode pairs that achieve maximum separability among different type of motor imagery activities in Table 10. We observed that on the BCI Competition-III dataset, all synchronization measures identified couplings between similar group of electrode pairs. However, on the PhysioNet dataset, the groups of electrode pairs identified to be in synchrony differed for the different synchronization measures. While this makes the interpretation of identified couplings challenging meaningful comparisons can still be made as follows;

A first-look analysis on PhysioNet dataset (right fist versus left fist imagination) reveals that cosine-based similarity captured mostly the parietal-central electrode couplings, cross-correlation the parietal-parietal electrode couplings, nonlinear interdependency central-parietal electrode pairs, mutual information the frontal and parietal electrode couplings, correntropy the frontal electrode couplings and finally PLV the parietal-parietal electrode couplings.

As for the BCI Competition-III (right hand versus right foot

Table 10
The 5 most frequent electrode pairs obtained for both PhysioNet and BCI Competition datasets.

	Cosine-based	Cross Correlation	Nonlinear Int.	Correntropy	Mutual Information	PLV
PhysioNet Dataset	Fc3-P5	C6-AF3	C4-Po4	Fcz-Ft8	F5-F8	Tp8-Po7
	Fc6-Ft7	Cp3-Fp1	C6-Po4	F7-O1	Tp8-Po3	P5-P8
	C1-P7	Cp6-Po3	Cp5-O2	Fc1-Ft8	P8-Po7	P1-P8
	Cp5-P2	P5-P8	Cp1-Po4	Fcz-F8	Fc4-Tp8	Fc3-Ft7
	Cp6-Iz	P3-P8	Ft8-Po4	Fcz-Ft7	C5-F1	C4-P8
BCI Competition-III Dataset	Fc1-C1	Fc1-C1	Fc1-C1	Fc1-C1	Fc1-C1	CFC1-CCP3
	F3-CCP5	Fc1-CCP3	CFC1-Cp3	CFC1-Cp3	Fc1-CCP3	Cz-CCP3
	F1-CCP3	CFC1-CCP3	F7-CCP5	Cz-CP3	CFC1-CCP3	Fc1-CCP3
	F1-CCP5	Cz-CCP3	F5-CCP5	F1-CCP5	Cz-CCP3	Fcz-CCP3
	F1-Cp5	Cz-Cp1	FFC7-CCP5	F1-CCP3	Cz-Cp1	FFC1-CCP3

imagination), we observed that all synchronization measures consistently captured the left fronto central-central, left central-centro parietal and left fronto central-centro parietal connectivity. By taking both results into consideration, mutual information method can better unveil motor imagery task related connectivity patterns than the other synchronization methods. These electrode couplings result for each dataset shows that, for both datasets, mutual information can better unveil motor imagery task related connectivity patterns than the other synchronization measures.

For the right/left fist motor imagery task, mutual information captured the synchronization patterns that reflect the functional connectivity of left premotor area-right premotor area, supplementary motor area-left sensorimotor cortex, right premotor area-right sensorimotor cortex and right-left parietal regions. In the literature, these brain regions have already been identified to be strongly associated with hand motor imagery tasks. While the right and left premotor areas are responsible for the integration and processing of information collected from other regions of the brain [125,126], sensorimotor cortex plays a role in spatial control and motor planning [127]. In Ref. [128], authors found that both sensorimotor cortices and premotor area are simultaneously activated with supplementary motor area during hand motor imagery activity. In a later study, the same group identified connectivity patterns between similar regions for right- and left-hand motor imagery task [129].

Cognitive, sensory and motor functions require interconnectivity of anatomically as well as functionally different regions of the brain [130]. Basically, these regions reciprocally process and exchange neural information for each specific brain activity [131]. So far, in the literature, a great deal of brain activity recognition/characterization studies analyzed and used power-based features of electrophysiological data obtained from focal cortical activity of the brain with notable success [31,32,123,124]. However, as also depicted in many other studies, a complete assessment of brain function requires a detailed evaluation of the interaction between electrophysiological data collected from distinct regions of the brain [57,65,132]. Indeed, this perspective forms the main premise of the current study.

Yet, for a more concrete comparison of CSP-based power features and synchronization-based features, it may be helpful to recognize that, CSP essentially calculates the power of the latent channels obtained as weighted linear combinations of actual EEG signals. In case where synchronization occurs through concurrent power increase or decrease that is preserved through the prescribed linear weighting by the CSP, the resulting power features can be expected to be useful for task recognition. However, there is no clear indication on how synchrony manifests between different brain regions during tasks of interest. This, in fact, was the main reason for evaluating a battery of potential synchronization measures in a cognitive task recognition scenario in this manuscript. Consequently, CSP-based power features may be insensitive to synchronization modes that do not survive weighted linear average over a large number of brain regions, that may also explain their apparent weakness in the recognition problem considered here.

For right fist/left fist motor imagery recognition, performances obtained from a *priori* selected channel pairs show that the channel pairs proposed by Krusienski et al. [61] generally achieves better accuracy than the other ones. From a biophysical point of view, these channel pairs constitute inter- and intra-hemispheric connections and collect brain activity from premotor, primary motor, sensorimotor and central-parietal areas. In the literature, these brain areas are listed among the critical brain for regions and constitute the functional network related with the right/left hand/finger motor imagination tasks [125]. In line with the previous studies that examine the intra- and inter-hemispheric interactions, stated that these electrodes mainly manifest the electrical activity of parietal, central and premotor regions during right and left hand motor imagination [129,133]. A study accomplished by L. A. Wheaton et al. further stated that the increase of synchronization between premotor and parietal cortices are the signature of motor preparation task for praxis hand movements [134]. Since right/left fist imagination is not a fully praxis movement, it is reasonable to expect that these channel pairs demonstrate better recognition performance than the other ones. Another study that evaluates the functional networks during finger tapping imagination identified eight connections that are mainly observed between premotor and motor cortices [125]. Yet, the results in Tables 3 and 4 show that automatically selected channel pairs outperform these a *priori* determined channel pairs for imaginary motor activity recognition. Clearly, the issue of which channel pairs are useful for which activity is to be elucidated further. One possible avenue of research may be to evaluate which channel pairs are often selected across the subjects of a large cohort. The current study forms the initial stage of a funded project that addresses a connectivity-based brain activity characterization. In the later stage of this project, we are currently seeking to capture the synchronization patterns that emerge in a short time window during the cognitive task in different time lags as well as in different latency values. This, however, entails a 3-parameter optimization with additional algorithmic and computational challenges and is under preparation for a follow-up paper.

5. Conclusions

In this study, we applied several synchronization measures in a novel cognitive task recognition framework. We characterized the brain activity by means of calculating the synchronization between channels at task-specific time lags. To this end, we applied several synchronization measures and calculated the characteristic time lags (task specific time lags) associated with different cognitive tasks: mutual information, correntropy, phase locking value, cross-correlation, nonlinear interdependence and cosine-based similarity. In the training phase, the task-specific time lags were obtained and used for constructing training feature vectors. These lags maximized the average synchronization for their respective channel pairs and cognitive task types in the training set. In the test phase, we calculated the synchronization values at the same task-specific time lags calculated in the training phase and constructed the test feature vectors. Due to the high dimensionality of the feature vectors, we carried out a feature selection using Fisher ratio along with a

priori suggested channel pairs in the literature. For recognition, we used a FLD classifier. The results in Tables 3 and 4 show that the recognition rates were below the minimum reliable communication rate (i.e. %70) for PhysioNet dataset [135]. However, for the BCI Competition-III dataset, the average performance varied between %69-%76.

Performance evaluation was carried out using a realistic cross validation scheme that uses a chronological partitioning of the data into training and testing sets. In classification results on the PhysioNet Motor Movement/Imagery Dataset, connectivity-based framework evaluated here outperformed a CSP-based benchmark scheme. Using BCI Competition-III dataset, it achieved a slightly lower performance than the CSP method. These results indicate that task-specific inter-regional lagged synchronization between potentially remote brain regions were used effectively to discriminate between different motor imagery tasks and is important to estimate the directions of information flow during cognitive tasks.

For future studies, the brain connectivity methodology adopted in this work can be useful in a real-time asynchronous cognitive task identification framework. Since the synchronous type methods calculate relevant features in a pre-determined time window, the asynchronous version needs to monitor the changes in brain activity in flowing EEG data to capture the status change as quickly as possible. In addition, synchronization profiles among different channel pairs offer the potential to discriminate between a great number of sensory, cognitive or motor tasks, as the number of pair sets increase geometrically with the number of EEG channels. Consequently, with further improvements, a brain connectivity-based approach can lead to a reliable, robust analysis method for online BCI applications.

Conflicts of interest

None Declared.

Acknowledgement

This study was supported by a grant awarded to Dr. Bilge KARAÇALI by The Scientific and Technological Research Council of Turkey (TUBITAK) with grant number 117E784.

References

[1] C. Güdücü, B.O. Olcay, L. Schäfer, M. Aziz, V.A. Schriever, M. Özgören, T. Hummel, Separating normosmic and anosmic patients based on entropy evaluation of olfactory event-related potentials, Brain Res. 1708 (2019) 78–83, https://doi.org/10.1016/j.brainres.2018.12.012.
[2] B. Koley, D. Dey, An ensemble system for automatic sleep stage classification using single channel EEG signal, Comput. Biol. Med. 42 (2012) 1186–1195, https://doi.org/10.1016/j.compbiomed.2012.09.012.
[3] A. Asif, M. Majid, S.M. Anwar, Human stress classification using EEG signals in response to music tracks, Comput. Biol. Med. 107 (2019) 182–196, https://doi.org/10.1016/j.compbiomed.2019.02.015.
[4] J.R. Wolpaw, N. Birbaumer, D.J. McFarland, G. Pfurtscheller, T.M. Vaughan, Brain–computer interfaces for communication and control, Clin. Neurophysiol. 113 (2002) 767–791. https://doi.org/10.1016/S1388-2457(02)00057-3.
[5] R.A. Ramadan, A.V. Vasilakos, Brain computer interface: control signals review, Neurocomputing 223 (2017) 26–44, https://doi.org/10.1016/j.neucom.2016.10.024.
[6] U. Chaudhary, N. Birbaumer, A. Ramos-Murguialday, Brain-computer interfaces for communication and rehabilitation, Nat. Rev. Neurol. 12 (2016) 513–525, https://doi.org/10.1038/nrneurol.2016.113.
[7] L.A. Farwell, E. Donchin, Talking off the top of your head: toward a mental prosthesis utilizing event-related brain potentials, Electroencephalogr. Clin. Neurophysiol. 70 (1988) 510–523, https://doi.org/10.1016/0013-4694(88)90149-6.
[8] C.C. Postelnicu, D. Talaba, P300-based brain-neuronal computer interaction for spelling applications, IEEE Trans. Biomed. Eng. 60 (2013) 534–543, https://doi.org/10.1109/TBME.2012.2228645.
[9] H. Yuan, B. He, Brain-computer interfaces using sensorimotor rhythms: current state and future perspectives, IEEE Trans. Biomed. Eng. 61 (2014) 1425–1435, https://doi.org/10.1109/TBME.2014.2312397.
[10] L. Bai, T. Yu, Y. Li, A brain computer interface-based explorer, J. Neurosci. Methods 244 (2015) 2–7, https://doi.org/10.1016/j.jneumeth.2014.06.015.
[11] T. Yu, Y. Li, J. Long, Z. Gu, Surfing the internet with a BCI mouse, J. Neural Eng. 9 (2012), https://doi.org/10.1088/1741-2560/9/3/036012.
[12] S. Dodia, D.R. Edla, A. Bablani, D. Ramesh, V. Kuppili, An efficient EEG based deceit identification test using wavelet packet transform and linear discriminant analysis, J. Neurosci. Methods 314 (2019) 31–40, https://doi.org/10.1016/j.jneumeth.2019.01.007.
[13] J.S. Kang, U. Park, V. Gonuguntla, K.C. Veluvolu, M. Lee, Human implicit intent recognition based on the phase synchrony of EEG signals, Pattern Recognit. Lett. 66 (2015) 144–152, https://doi.org/10.1016/j.patrec.2015.06.013.
[14] H.G. Jo, J.Y. Park, C.K. Lee, S.K. An, S.K. Yoo, Genetic fuzzy classifier for sleep stage identification, Comput. Biol. Med. 40 (2010) 629–634, https://doi.org/10.1016/j.compbiomed.2010.04.007.
[15] X.S. Zhang, R.J. Roy, E.W. Jensen, EEG complexity as a measure of depth of anesthesia for patients, IEEE Trans. Biomed. Eng. 48 (2001) 1424–1433, https://doi.org/10.1109/10.966601.
[16] R. San-Segundo, M. Gil-Martín, L.F. D'Haro-Enríquez, J.M. Pardo, Classification of epileptic EEG recordings using signal transforms and convolutional neural networks, Comput. Biol. Med. 109 (2019) 148–158, https://doi.org/10.1016/j.compbiomed.2019.04.031.
[17] P. Mirowski, D. Madhavan, Y. LeCun, R. Kuzniecky, Classification of patterns of EEG synchronization for seizure prediction, Clin. Neurophysiol. 120 (2009) 1927–1940, https://doi.org/10.1016/j.clinph.2009.09.002.
[18] R. Hussein, H. Palangi, R.K. Ward, Z.J. Wang, Optimized deep neural network architecture for robust detection of epileptic seizures using EEG signals, Clin. Neurophysiol. 130 (2019) 25–37, https://doi.org/10.1016/j.clinph.2018.10.010.
[19] S. Dutta, M. Singh, A. Kumar, Classification of non-motor cognitive task in EEG based brain-computer interface using phase space features in multivariate empirical mode decomposition domain, Biomed. Signal Process. Control 39 (2018) 378–389, https://doi.org/10.1016/j.bspc.2017.08.004.
[20] M. Besserve, M. Philippe, G. Florence, F. Laurent, L. Garnero, J. Martinerie, Prediction of performance level during a cognitive task from ongoing EEG oscillatory activities, Clin. Neurophysiol. 119 (2008) 897–908, https://doi.org/10.1016/j.clinph.2007.12.003.
[21] F. Lotte, M. Congedo, A. Lécuyer, F. Lamarche, B. Arnaldi, A review of classification algorithms for EEG-based brain-computer interfaces, J. Neural Eng. 4 (2007), https://doi.org/10.1088/1741-2560/4/2/R01.
[22] T. Carlson, L. Tonin, S. Perdikis, R. Leeb, J.D.R. Millan, A hybrid BCI for enhanced control of a telepresence robot, in: Proc. Annu. Int. Conf. IEEE Eng. Med. Biol. Soc. EMBS, Institute of Electrical and Electronics Engineers Inc., 2013, pp. 3097–3100, https://doi.org/10.1109/EMBC.2013.6610196.
[23] K. Lafleur, K. Cassady, A. Doud, K. Shades, E. Rogin, B. He, Quadcopter control in three-dimensional space using a noninvasive motor imagery-based brain-computer interface, J. Neural Eng. 10 (2013), https://doi.org/10.1088/1741-2560/10/4/046003.
[24] A.J. Doud, J.P. Lucas, M.T. Pisansky, B. He, Continuous three-dimensional control of a virtual helicopter using a motor imagery based Brain-Computer interface, PLoS One 6 (2011), https://doi.org/10.1371/journal.pone.0026322.
[25] M. Pregenzer, G. Pfurtscheller, Frequency component selection for an EEG-based brain to computer interface, IEEE Trans. Rehabil. Eng. 7 (1999) 413–419, https://doi.org/10.1109/86.808944.
[26] D.J. McFarland, J.R. Wolpaw, Sensorimotor rhythm-based brain-computer interface (BCI): model order selection for autoregressive spectral analysis, J. Neural Eng. 5 (2008) 155–162, https://doi.org/10.1088/1741-2560/5/2/006.
[27] A. Schloegl, K. Lugger, G. Pfurtscheller, Using adaptive autoregressive parameters for a brain-computer-interface experiment, in: Annu. Int. Conf. IEEE Eng. Med. Biol. - Proc, 4, 1997, pp. 1533–1535, https://doi.org/10.1109/IEMBS.1997.757002.
[28] N. Firat Ince, S. Arica, A. Tewfik, Classification of single trial motor imagery EEG recordings with subject adapted non-dyadic arbitrary time-frequency tilings, J. Neural Eng. 3 (2006) 235–244, https://doi.org/10.1088/1741-2560/3/3/006.
[29] N.F. Ince, F. Goksu, A.H. Tewfik, S. Arica, Adapting subject specific motor imagery EEG patterns in space-time-frequency for a brain computer interface, Biomed. Signal Process. Control 4 (2009) 236–246, https://doi.org/10.1016/j.bspc.2009.03.005.
[30] L. Qin, B. He, A wavelet-based time-frequency analysis approach for classification of motor imagery for brain-computer interface applications, J. Neural Eng. 2 (2005) 65–72, https://doi.org/10.1088/1741-2560/2/4/001.
[31] H. Ramoser, J. Müller-Gerking, G. Pfurtscheller, Optimal spatial filtering of single trial EEG during imagined hand movement, IEEE Trans. Rehabil. Eng. 8 (2000) 441–446, https://doi.org/10.1109/86.895946.
[32] F. Lotte, C. Guan, Regularizing common spatial patterns to improve BCI designs: unified theory and new algorithms, IEEE Trans. Biomed. Eng. 58 (2011) 355–362, https://doi.org/10.1109/TBME.2010.2082539.
[33] S.H. Park, D. Lee, S.G. Lee, Filter bank regularized common spatial pattern ensemble for small sample motor imagery classification, IEEE Trans. Neural Syst. Rehabil. Eng. 26 (2018) 498–505, https://doi.org/10.1109/TNSRE.2017.2757519.
[34] A. Tzovara, M.M. Murray, G. Plomp, M.H. Herzog, C.M. Michel, M. De Lucia, Decoding stimulus-related information from single-trial EEG responses based on voltage topographies, Pattern Recognit. 45 (2012) 2109–2122, https://doi.org/10.1016/j.patcog.2011.04.007.
[35] C. Vidaurre, N. Krämer, B. Blankertz, A. Schlögl, Time domain parameters as a feature for EEG-based brain-computer interfaces, Neural Netw. 22 (2009) 1313–1319, https://doi.org/10.1016/j.neunet.2009.07.020.

[36] A.M. Bastos, J.-M. Schoffelen, A tutorial review of functional connectivity analysis methods and their interpretational pitfalls, Front. Syst. Neurosci. 9 (2016) 175.
[37] D. Meunier, R. Lambiotte, E.T. Bullmore, Modular and hierarchically modular organization of brain networks, Front. Neurosci. 4 (2010), https://doi.org/10.3389/fnins.2010.00200.
[38] C. Zhou, L. Zemanová, G. Zamora, C.C. Hilgetag, J. Kurths, Hierarchical organization unveiled by functional connectivity in complex brain networks, Phys. Rev. Lett. 97 (2006), https://doi.org/10.1103/PhysRevLett.97.238103.
[39] A.A. Fingelkurts, A.A. Fingelkurts, S. Kähkönen, Functional connectivity in the brain - is it an elusive concept? Neurosci. Biobehav. Rev. 28 (2005) 827–836, https://doi.org/10.1016/j.neubiorev.2004.10.009.
[40] C.J. Stam, E.C.W. van Straaten, The organization of physiological brain networks, Clin. Neurophysiol. 123 (2012) 1067–1087, https://doi.org/10.1016/j.clinph.2012.01.011.
[41] S. Sargolzaei, M. Cabrerizo, M. Goryawala, A.S. Eddin, M. Adjouadi, Scalp EEG brain functional connectivity networks in pediatric epilepsy, Comput. Biol. Med. 56 (2015) 158–166, https://doi.org/10.1016/j.compbiomed.2014.10.018.
[42] L. Faes, D. Marinazzo, G. Nollo, A. Porta, An information-theoretic framework to map the spatiotemporal dynamics of the scalp electroencephalogram, IEEE Trans. Biomed. Eng. 63 (2016) 2488–2496, https://doi.org/10.1109/TBME.2016.2569823.
[43] J. Jeong, J.C. Gore, B.S. Peterson, Mutual information analysis of the EEG in patients with Alzheimer's disease, Clin. Neurophysiol. 112 (2001) 827–835, https://doi.org/10.1016/S1388-2457(01)00513-2.
[44] E. Olejarczyk, L. Marzetti, V. Pizzella, F. Zappasodi, Comparison of connectivity analyses for resting state EEG data, J. Neural Eng. 14 (2017), https://doi.org/10.1088/1741-2552/aa6401.
[45] B.O. Olcay, B. Karacali, M. Ozgoren, C. Guducu, Brain activity characterization by entropic clustering of EEG signals, in: Institute of Electrical and Electronics Engineers (IEEE), 2017, pp. 1–4, https://doi.org/10.1109/siu.2017.7960503.
[46] A. Wilmer, M. de Lussanet, M. Lappe, Time-delayed mutual information of the phase as a measure of functional connectivity, PLoS One 7 (2012), https://doi.org/10.1371/journal.pone.0044633.
[47] M. Wibral, N. Pampu, V. Priesemann, F. Siebenhühner, H. Seiwert, M. Lindner, J. T. Lizier, R. Vicente, Measuring information-transfer delays, PLoS One 8 (2013), e55809. https://doi.org/10.1371/journal.pone.0055809.
[48] M. Lobier, F. Siebenhühner, S. Palva, J.M. Palva, Phase transfer entropy: a novel phase-based measure for directed connectivity in networks coupled by oscillatory interactions, Neuroimage 85 (2014) 853–872, https://doi.org/10.1016/j.neuroimage.2013.08.056.
[49] X. Wan, B. Crüts, H.J. Jensen, The causal inference of cortical neural networks during music improvisations, PLoS One 9 (2014), https://doi.org/10.1371/journal.pone.0112776.
[50] J.W. Xu, H. Bakardjian, A. Cichocki, J.C. Principe, A new nonlinear similarity measure for multichannel biological signals, in: IEEE Int. Conf. Neural Networks - Conf. Proc, 2007, pp. 2046–2051, https://doi.org/10.1109/IJCNN.2007.4371273.
[51] L. Li, I.M. Park, S. Seth, J.C. Sanchez, J.C. Príncipe, Functional connectivity dynamics among cortical neurons: a dependence analysis, IEEE Trans. Neural Syst. Rehabil. Eng. 20 (2012) 18–30, https://doi.org/10.1109/TNSRE.2011.2176749.
[52] B. Fadlallah, S. Seth, A. Keil, J. Principe, Quantifying cognitive state from EEG using dependence measures, IEEE Trans. Biomed. Eng. 59 (2012) 2773–2781, https://doi.org/10.1109/TBME.2012.2210283.
[53] S. Aviyente, E.M. Bernat, W.S. Evans, S.R. Sponheim, A phase synchrony measure for quantifying dynamic functional integration in the brain, Hum. Brain Mapp. 32 (2011) 80–93, https://doi.org/10.1002/hbm.21000.
[54] C.J. Stam, G. Nolte, A. Daffertshofer, Phase lag index: assessment of functional connectivity from multi channel EEG and MEG with diminished bias from common sources, Hum. Brain Mapp. 28 (2007) 1178–1193, https://doi.org/10.1002/hbm.20346.
[55] S. Khanmohammadi, An improved synchronization likelihood method for quantifying neuronal synchrony, Comput. Biol. Med. 91 (2017) 80–95, https://doi.org/10.1016/j.compbiomed.2017.09.022.
[56] H. Bakhshayesh, S.P. Fitzgibbon, A.S. Janani, T.S. Grummett, K.J. Pope, Detecting synchrony in EEG: a comparative study of functional connectivity measures, Comput. Biol. Med. 105 (2019) 1–15, https://doi.org/10.1016/j.compbiomed.2018.12.005.
[57] V. Sakkalis, Review of advanced techniques for the estimation of brain connectivity measured with EEG/MEG, Comput. Biol. Med. 41 (2011) 1110–1117, https://doi.org/10.1016/j.compbiomed.2011.06.020.
[58] E. Pereda, R.Q. Quiroga, J. Bhattacharya, Nonlinear multivariate analysis of neurophysiological signals, Prog. Neurobiol. 77 (2005) 1–37, https://doi.org/10.1016/j.pneurobio.2005.10.003.
[59] J. Dauwels, F. Vialatte, T. Musha, A. Cichocki, A comparative study of synchrony measures for the early diagnosis of Alzheimer's disease based on EEG, Neuroimage 49 (2010) 668–693, https://doi.org/10.1016/j.neuroimage.2009.06.056.
[60] J.D. Bonita, L.C.C. Ambolode, B.M. Rosenberg, C.J. Cellucci, T.A.A. Watanabe, P. E. Rapp, A.M. Albano, Time domain measures of inter-channel EEG correlations: a comparison of linear, nonparametric and nonlinear measures, Cogn. Neurodyn. 8 (2014) 1–15, https://doi.org/10.1007/s11571-013-9267-8.
[61] D.J. Krusienski, D.J. McFarland, J.R. Wolpaw, Value of amplitude, phase, and coherence features for a sensorimotor rhythm-based brain-computer interface, Brain Res. Bull. 87 (2012) 130–134, https://doi.org/10.1016/j.brainresbull.2011.09.019.
[62] M. Hamedi, S.H. Salleh, A.M. Noor, Electroencephalographic motor imagery brain connectivity analysis for BCI: a review, Neural Comput. 28 (2016) 999–1041, https://doi.org/10.1162/NECO_a_00838.
[63] I. Daly, S.J. Nasuto, K. Warwick, Brain computer interface control via functional connectivity dynamics, Pattern Recognit. 45 (2012) 2123–2136, https://doi.org/10.1016/j.patcog.2011.04.034.
[64] V. Gonuguntla, Y. Wang, K.C. Veluvolu, Event-related functional network identification: application to EEG classification, IEEE J. Sel. Top. Signal Process. 10 (2016) 1284–1294, https://doi.org/10.1109/JSTSP.2016.2602007.
[65] D. La Rocca, P. Campisi, B. Vegso, P. Cserti, G. Kozmann, F. Babiloni, F. De Vico Fallani, Human brain distinctiveness based on EEG spectral coherence connectivity, IEEE Trans. Biomed. Eng. 61 (2014) 2406–2412, https://doi.org/10.1109/TBME.2014.2317881.
[66] S. Siuly, Y. Li, Improving the separability of motor imagery EEG signals using a cross correlation-based least square support vector machine for brain-computer interface, IEEE Trans. Neural Syst. Rehabil. Eng. 20 (2012) 526–538, https://doi.org/10.1109/TNSRE.2012.2184838.
[67] B.R. Hermanto, T.R. Mengko, A. Indrayanto, A.S. Prihatmanto, Brain signal reference concept using cross correlation based for brain computer interface, in: Proc. 2013 3rd Int. Conf. Instrumentation, Commun. Inf. Technol., Biomed. Eng. Sci. Technol. Improv. Heal. Safety, Environ., ICICI-BME 2013, IEEE Computer Society, 2013, pp. 388–391, https://doi.org/10.1109/ICICI-BME.2013.6698531.
[68] C.G. Rong, D. Xiaoning, From Chaos to Order: Methodologies, Perspectives and Applications, World Scientific, 1998.
[69] E.M. Shahverdiev, S. Sivaprakasam, K.A. Shore, Lag synchronization in time-delayed systems, Phys. Lett. Sect. A Gen. At. Solid State Phys. 292 (2002) 320–324, https://doi.org/10.1016/S0375-9601(01)00824-6.
[70] O. Sporns, G. Tononi, G.M. Edelman, Connectivity and complexity: the relationship between neuroanatomy and brain dynamics, Neural Netw. 13 (2000) 909–922, https://doi.org/10.1016/S0893-6080(00)00053-8.
[71] M. Wibral, B. Rahm, M. Rieder, M. Lindner, R. Vicente, J. Kaiser, Transfer entropy in magnetoencephalographic data: quantifying information flow in cortical and cerebellar networks, Prog. Biophys. Mol. Biol. 105 (2011) 80–97, https://doi.org/10.1016/j.pbiomolbio.2010.11.006.
[72] N.C. Pampu, R. Vicente, R.C. Muresan, V. Priesemann, F. Siebenhuhner, M. Wibral, Transfer entropy as a tool for reconstructing interaction delays in neural signals, in: ISSCS 2013 - Int. Symp. Signals, Circuits Syst, 2013, https://doi.org/10.1109/ISSCS.2013.6651210.
[73] S.H. Na, S.H. Jin, S.Y. Kim, B.J. Ham, EEG in schizophrenic patients: mutual information analysis, Clin. Neurophysiol. 113 (2002) 1954–1960, https://doi.org/10.1016/S1388-2457(02)00197-9.
[74] J. Gotman, Measurement of small time differences between EEG channels: method and application to epileptic seizure propagation, Electroencephalogr. Clin. Neurophysiol. 56 (1983) 501–514, https://doi.org/10.1016/0013-4694(83)90235-3.
[75] P.Y. Ktonas, R. Mallart, Estimation of time delay between EEG signals for epileptic focus localization: statistical error considerations, Electroencephalogr. Clin. Neurophysiol. 78 (1991) 105–110, https://doi.org/10.1016/0013-4694(91)90109-H.
[76] R. van Bergen, A Discrete Mutual Information Estimator of Continuous Signals, 1986.
[77] P.H. Boeijinga, F.H. Lopes da Silva, A new method to estimate time delays between EEG signals applied to beta activity of the olfactory cortical areas, Electroencephalogr. Clin. Neurophysiol. 73 (1989) 198–205, https://doi.org/10.1016/0013-4694(89)90120-X.
[78] A. Adhikari, T. Sigurdsson, M.A. Topiwala, J.A. Gordon, Cross-correlation of instantaneous amplitudes of field potential oscillations: a straightforward method to estimate the directionality and lag between brain areas, J. Neurosci. Methods 191 (2010) 191–200, https://doi.org/10.1016/j.jneumeth.2010.06.019.
[79] B. Blankertz, K.R. Müller, D.J. Krusienski, G. Schalk, J.R. Wolpaw, A. Schlögl, G. Pfurtscheller, J.D.R. Millán, M. Schröder, N. Birbaumer, The BCI competition III: validating alternative approaches to actual BCI problems, IEEE Trans. Neural Syst. Rehabil. Eng. 14 (2006) 153–159, https://doi.org/10.1109/TNSRE.2006.875642.
[80] G. Dornhege, B. Blankertz, G. Curio, K.R. Müller, Boosting bit rates in noninvasive EEG single-trial classifications by feature combination and multiclass paradigms, IEEE Trans. Biomed. Eng. 51 (2004) 993–1002, https://doi.org/10.1109/TBME.2004.827088.
[81] A.L. Goldberger, L.A. Amaral, L. Glass, J.M. Hausdorff, P.C. Ivanov, R.G. Mark, J. E. Mietus, G.B. Moody, C.K. Peng, H.E. Stanley, PhysioBank, PhysioToolkit, and PhysioNet: components of a new research resource for complex physiologic signals, Circulation 101 (2000). https://www.ahajournals.org/doi/abs/10.1161/circ.101.23.e215. (Accessed 13 September 2019).
[82] G. Schalk, D.J. McFarland, T. Hinterberger, N. Birbaumer, J.R. Wolpaw, BCI2000: a general-purpose brain-computer interface (BCI) system, IEEE Trans. Biomed. Eng. 51 (2004) 1034–1043, https://doi.org/10.1109/TBME.2004.827072.
[83] F. Lotte, Study of Electroencephalographic signal processing and classification techniques towards the use of Brain-Computer interfaces in virtual reality applications. https://tel.archives-ouvertes.fr/tel-00356346v2, 2008. (Accessed 13 September 2019).
[84] D.J. McFarland, L.M. McCane, S.V. David, J.R. Wolpaw, Spatial filter selection for EEG-based communication, Electroencephalogr. Clin. Neurophysiol. 103 (1997) 386–394, https://doi.org/10.1016/S0013-4694(97)00022-2.

[85] R.A. FISHER, The use OF multiple measurements IN taxonomic problems, Ann. Eugen. 7 (1936) 179–188, https://doi.org/10.1111/j.1469-1809.1936.tb02137.x.
[86] I. Park, J.C. Príncipe, Correntropy based Granger causality, in: ICASSP, IEEE Int. Conf. Acoust. Speech Signal Process. - Proc, 2008, pp. 3605–3608, https://doi.org/10.1109/ICASSP.2008.4518432.
[87] C.E. Shannon, W. Weaver, A Mathematical Theory of Communication, University of Illinois Press, Champaign, IL, USA, 1963.
[88] J.P. Lachaux, E. Rodriguez, J. Martinerie, F.J. Varela, Measuring phase synchrony in brain signals, Hum. Brain Mapp. 8 (1999) 194–208, https://doi.org/10.1002/(SICI)1097-0193(1999)8:4<194::AID-HBM4>3.0.CO;2-C.
[89] J. Arnhold, P. Grassberger, K. Lehnertz, C.E. Elger, A robust method for detecting interdependences: application to intracranially recorded EEG, Phys. D Nonlinear Phenom. 134 (1999) 419–430, https://doi.org/10.1016/S0167-2789(99)00140-2.
[90] W. Liu, P.P. Pokharel, J.C. Principe, Correntropy: properties and applications in non-Gaussian signal processing, IEEE Trans. Signal Process. 55 (2007) 5286–5298, https://doi.org/10.1109/TSP.2007.896065.
[91] M. Rao, S. Seth, J. Xu, Y. Chen, H. Tagare, J.C. Príncipe, A test of independence based on a generalized correlation function, Signal Process. 91 (2011) 15–27, https://doi.org/10.1016/j.sigpro.2010.06.002.
[92] A. Kraskov, H. Stögbauer, P. Grassberger, Estimating mutual information, Phys. Rev. E Stat. Phys. Plasmas Fluids Relat. Interdiscip. Top. 69 (2004) 16, https://doi.org/10.1103/PhysRevE.69.066138.
[93] C. Brunner, R. Scherer, B. Graimann, G. Supp, G. Pfurtscheller, Online control of a brain-computer interface using phase synchronization, IEEE Trans. Biomed. Eng. 53 (2006) 2501–2506, https://doi.org/10.1109/TBME.2006.881775.
[94] C. Bandt, B. Pompe, Permutation entropy: a natural complexity measure for time series, Phys. Rev. Lett. 88 (2002) 4, https://doi.org/10.1103/PhysRevLett.88.174102.
[95] R. Baravalle, O.A. Rosso, F. Montani, Causal Shannon-Fisher characterization of motor/imagery movements in EEG, Entropy 20 (2018), https://doi.org/10.3390/e20090660.
[96] R. Baravalle, O.A. Rosso, F. Montani, Rhythmic activities of the brain: quantifying the high complexity of beta and gamma oscillations during visuomotor tasks, Chaos 28 (2018), https://doi.org/10.1063/1.5025187.
[97] R.O. Duda, P.E. Hart, D.G. Stork, Pattern Classification, John Wiley & Sons, 2012.
[98] Q. Wei, Y. Wang, X. Gao, S. Gao, Amplitude and phase coupling measures for feature extraction in an EEG-based brain-computer interface, J. Neural Eng. 4 (2007) 120–129, https://doi.org/10.1088/1741-2560/4/2/012.
[99] Y. Wang, B. Hong, X. Gao, S. Gao, Phase synchrony measurement in motor cortex for classifying single-trial EEG during motor imagery, in: Annu. Int. Conf. IEEE Eng. Med. Biol. - Proc, 2006, pp. 75–78, https://doi.org/10.1109/IEMBS.2006.259673.
[100] D. Rathee, H. Cecotti, G. Prasad, Single-trial effective brain connectivity patterns enhance discriminability of mental imagery tasks, J. Neural Eng. 14 (2017), https://doi.org/10.1088/1741-2552/aa785c.
[101] M. Hamedi, S.H. Salleh, C.M. Ting, S.B. Samdin, A. Mohd Noor, Sensor space time-varying information flow analysis of multiclass motor imagery through Kalman Smoother and em algorithm, in: 2015 Int. Conf. BioSignal Anal. Process. Syst. ICBAPS 2015, Institute of Electrical and Electronics Engineers Inc., 2015, pp. 118–122, https://doi.org/10.1109/ICBAPS.2015.7292230.
[102] J.A. Gaxiola-Tirado, R. Salazar-Varas, D. Gutierrez, Using the partial directed coherence to assess functional connectivity in electroencephalography data for brain-computer interfaces, IEEE Trans. Cogn. Dev. Syst. 10 (2018) 776–783, https://doi.org/10.1109/TCDS.2017.2777180.
[103] G. Müller-Putz, R. Scherer, C. Brunner, R. Leeb, G. Pfurtscheller, Better than random: a closer look on BCI results, Int. J. Bioelectromagn. 10 (2008) 52–55.
[104] C. Park, C.C. Took, D.P. Mandic, Augmented complex common spatial patterns for classification of noncircular EEG from motor imagery tasks, IEEE Trans. Neural Syst. Rehabil. Eng. 22 (2014) 1–10, https://doi.org/10.1109/TNSRE.2013.2294903.
[105] Y. Kim, J. Ryu, K.K. Kim, C.C. Took, D.P. Mandic, C. Park, Motor imagery classification using mu and beta rhythms of EEG with strong uncorrelating transform based complex common spatial patterns, Comput. Intell. Neurosci. 2016 (2016) 1.
[106] V.S. Handiru, V.A. Prasad, Optimized Bi-objective EEG channel selection and cross-subject generalization with brain-computer interfaces, IEEE Trans. Human-Machine Syst. 46 (2016) 777–786, https://doi.org/10.1109/THMS.2016.2573827.
[107] M. Tolić, F. Jović, Classification of wavelet transformed EEG signals with neural network for imagined mental and motor tasks, Kinesiol. Int. J. Fundam. Appl. Kinesiol. 45 (2013) 130–138.
[108] M. Athif, H. Ren, WaveCSP: a robust motor imagery classifier for consumer EEG devices, Australas. Phys. Eng. Sci. Med. 42 (2019) 159–168, https://doi.org/10.1007/s13246-019-00721-0.
[109] C. Carvalhaes, J.A. De Barros, The surface Laplacian technique in EEG: theory and methods, Int. J. Psychophysiol. 97 (2015) 174–188, https://doi.org/10.1016/j.ijpsycho.2015.04.023.
[110] V. Vapnik, The Nature of Statistical Learning Theory, Springer science & business media, 2013.
[111] G.-B. Huang, L. Chen, C.K. Siew, Universal approximation using incremental constructive feedforward networks with random hidden nodes, IEEE Trans. Neural Netw. 17 (2006) 879–892.
[112] Y. Zhang, Y. Wang, G. Zhou, J. Jin, B. Wang, X. Wang, A. Cichocki, Multi-kernel extreme learning machine for EEG classification in brain-computer interfaces, Expert Syst. Appl. 96 (2018) 302–310, https://doi.org/10.1016/j.eswa.2017.12.015.
[113] Z. Jin, G. Zhou, D. Gao, Y. Zhang, EEG classification using sparse Bayesian extreme learning machine for brain–computer interface, Neural Comput. Appl. (2018), https://doi.org/10.1007/s00521-018-3735-3.
[114] H. Higashi, T. Tanaka, Simultaneous design of FIR filter banks and spatial patterns for EEG signal classification, IEEE Trans. Biomed. Eng. 60 (2013) 1100–1110, https://doi.org/10.1109/TBME.2012.2215960.
[115] K.K. Ang, Z.Y. Chin, H. Zhang, C. Guan, filter bank common spatial pattern (FBCSP) in brain-computer interface, in: Proc. Int. Jt. Conf. Neural Networks, 2008, pp. 2390–2397, https://doi.org/10.1109/IJCNN.2008.4634130.
[116] M. Goldhacker, A.M. Tomé, M.W. Greenlee, E.W. Lang, Frequency-resolved dynamic functional connectivity reveals scale-stable features of connectivity-states, Front. Hum. Neurosci. 12 (2018) 253, https://doi.org/10.3389/fnhum.2018.00253.
[117] S. Kumar, A. Sharma, T. Tsunoda, An improved discriminative filter bank selection approach for motor imagery EEG signal classification using mutual information, BMC Bioinf. 18 (2017), https://doi.org/10.1186/s12859-017-1964-6.
[118] R.Q. Quiroga, A. Kraskov, T. Kreuz, P. Grassberger, Performance of different synchronization measures in real data: a case study on electroencephalographic signals, Phys. Rev. E. 65 (2002) 41903.
[119] M.H. Wu, R.E. Frye, G. Zouridakis, A comparison of multivariate causality based measures of effective connectivity, Comput. Biol. Med. 41 (2011) 1132–1141, https://doi.org/10.1016/j.compbiomed.2011.06.007.
[120] A. Montalto, L. Faes, D. Marinazzo, MuTE: a matlab toolbox to compare established and novel estimators of the multivariate transfer entropy, PLoS One 9 (2014) 1–13, https://doi.org/10.1371/journal.pone.0109462.
[121] T. Schreiber, Measuring information transfer, Phys. Rev. Lett. 85 (2000) 461–464, https://doi.org/10.1103/PhysRevLett.85.461.
[122] Y. Jiao, Y. Zhang, X. Chen, E. Yin, J. Jin, X. Wang, A. Cichocki, Sparse group representation model for motor imagery EEG classification, IEEE J. Biomed. Heal. Informatics. 23 (2019) 631–641, https://doi.org/10.1109/JBHI.2018.2832538.
[123] Y. Zhang, G. Zhou, J. Jin, X. Wang, A. Cichocki, Optimizing spatial patterns with sparse filter bands for motor-imagery based brain-computer interface, J. Neurosci. Methods 255 (2015) 85–91, https://doi.org/10.1016/j.jneumeth.2015.08.004.
[124] Y. Zhang, C.S. Nam, G. Zhou, J. Jin, X. Wang, A. Cichocki, Temporally constrained sparse group spatial patterns for motor imagery BCI, IEEE Trans. Cybern. 49 (2019) 3322–3332, https://doi.org/10.1109/TCYB.2018.2841847.
[125] L. Xu, H. Zhang, M. Hui, Z. Long, Z. Jin, Y. Liu, L. Yao, Motor execution and motor imagery: a comparison of functional connectivity patterns based on graph theory, Neuroscience 261 (2014) 184–194, https://doi.org/10.1016/j.neuroscience.2013.12.005.
[126] G. Luppino, G. Rizzolatti, The organization of the frontal motor cortex, Physiology 15 (2000) 219–224.
[127] C.A. Porro, M.P. Francescato, V. Cettolo, M.E. Diamond, P. Baraldi, C. Zuiani, M. Bazzocchi, P.E. Di Prampero, Primary motor and sensory cortex activation during motor performance and motor imagery: a functional magnetic resonance imaging study, J. Neurosci. 16 (1996) 7688–7698.
[128] H. Chen, Q. Yang, W. Liao, Q. Gong, S. Shen, Evaluation of the effective connectivity of supplementary motor areas during motor imagery using Granger causality mapping, Neuroimage 47 (2009) 1844–1853, https://doi.org/10.1016/j.neuroimage.2009.06.026.
[129] Q. Gao, X. Duan, H. Chen, Evaluation of effective connectivity of motor areas during motor imagery and execution using conditional Granger causality, Neuroimage 54 (2011) 1280–1288, https://doi.org/10.1016/j.neuroimage.2010.08.071.
[130] Y. Gao, H. Su, R. Li, Y. Zhang, Synchronous analysis of brain regions based on multi-scale permutation transfer entropy, Comput. Biol. Med. 109 (2019) 272–279, https://doi.org/10.1016/j.compbiomed.2019.04.038.
[131] D. Rangaprakash, Connectivity analysis of multichannel EEG signals using recurrence based phase synchronization technique, Comput. Biol. Med. 46 (2014) 11–21, https://doi.org/10.1016/j.compbiomed.2013.10.025.
[132] R.E. Greenblatt, M.E. Pflieger, A.E. Ossadtchi, Connectivity measures applied to human brain electrophysiological data, J. Neurosci. Methods 207 (2012) 1–16, https://doi.org/10.1016/j.jneumeth.2012.02.025.
[133] A. Solodkin, P. Hlustik, E.E. Chen, S.L. Small, Fine modulation in network activation during motor execution and motor imagery, Cereb. Cortex 14 (2004) 1246–1255.
[134] L.A. Wheaton, G. Nolte, S. Bohlhalter, E. Fridman, M. Hallett, Synchronization of parietal and premotor areas during preparation and execution of praxis hand movements, Clin. Neurophysiol. 116 (2005) 1382–1390, https://doi.org/10.1016/j.clinph.2005.01.008.
[135] M. Ahn, S.C. Jun, Performance variation in motor imagery brain-computer interface: a brief review, J. Neurosci. Methods 243 (2015) 103–110, https://doi.org/10.1016/j.jneumeth.2015.01.033.

B. Orkan Olcay has received the B.Sc. on Electrical and Electronics Engineering from Çukurova University, Adana, in 2011. He received his M.Sc. on Electrical and Electronics Engineering from Izmir Institute of Technology, Izmir, 2014. He is now working as a research assistant in the Department of Electrical and Electronics Engineering, Izmir Institute of Technology, Izmir, Turkey. His research interests include Brain Dynamics, Complex Brain Networks, Brain-Computer Interfaces, Biomedical Signal Processing.

Bilge Karaçalı has received his BS on Electrical and Electronics Engineering from Bilkent University, and MS and PhD on Electrical Engineering from the North Carolina State University in 1999 and 2002. He worked as a postdoctoral research fellow in the Radiology Department of the School of Medicine, University of Pennsylvania. He joined the school of Biomedical Engineering, Science and Health Systems at Drexel University in 2005 as a research assistant professor and the assistant director of bioimaging of the Center of Integrated Bioinformatics. He is currently with the Electrical and Electronics Engineering Department at Izmir Institute of Technology as a full professor. He is director of the Biomedical Information Processing Laboratory.